Journal of Physics: Conference Series

PAPER • **OPEN ACCESS**

Vortex states near absolute zero in a weak-pinning amorphous Mo_xGe_{1-x} film probed by pulsed mode-locking resonance

To cite this article: N Sohara *et al* 2017 *J. Phys.: Conf. Ser.* **871** 012022

IOP Conf. Series: Journal of Physics: Conf. Series **871** (2017) 012022 doi:10.1088/1742-6596/871/1/012022

Vortex states near absolute zero in a weak-pinning amorphous Mo_xGe_{1-x} film probed by pulsed mode-locking resonance

N Sohara[1], A Ochi[1], E Murakami[1], K Ienaga[1], S Kaneko[1], N Kokubo[2] and S Okuma[1]

[1]Department of Physics, Tokyo Institute of Technology, 2-12-1, Ohokayama, Meguro-ku, Tokyo 152-8551, Japan

[2]Department of Engineering Science, The University of Electro-Communications, 1-5-1 Chofugaoka, Chofu, Tokyo 182-8585, Japan

E-mail: `sokuma@o.cc.titech.ac.jp`

Abstract. We have developed measurements of the mode-locking (ML) resonance with pulsed currents, which generates much less heat than the conventional one with continuous currents. Here, we present the experimental details of the pulsed ML measurement. Using this technique, we have succeeded in determining the dynamic melting field of a driven vortex lattice for a weak-pinning thick amorphous Mo_xGe_{1-x} film down to 0.05 K. We construct an *ideal* vortex phase diagram in the *absence* of pinning near zero temperature as a function of magnetic field.

1. Introduction

Since the discovery of high-T_c cuprates, equilibrium vortex states in the field-temperature ($B-T$) plane have been thoroughly studied. While melting of the vortex lattice with increasing T and B has been well established, the true vortex-lattice melting in the limit of $T = 0$, which is induced by strong quantum fluctuations [1-17], remains unclarified despite its fundamental significance. Part of the reason is that the pinning effect unavoidably contained in actual samples gives rise to the order-disorder transition from the ordered (or weakly disordered) vortex-lattice phase (OP) to the disordered vortex-glass phase (DP) [18-20]. This is associated with the peak effect at B_p, where B_p is determined from a peak in the depinning current [21-27]. The emergence of DP masks the observation of the true melting transition of the vortex lattice. To overcome this difficulty, in our earlier work we have performed the measurement of the mode-locking (ML) resonance [28-38], which enables to probe melting of the moving lattice decoupled from the underlying pinning potential [28-30,39-41].

However, the ML measurement could not be carried out at low enough T, e.g., $T < 1$ K, because the fast vortex motion generates more heat than the conventional transport measurement. Quite recently, we have developed the *pulsed* ML measurement that generates much less average heat, by three orders of magnitude, than the conventional one [42]. In this paper, we present the experimental details of the pulsed ML measurement. Hopefully, this method will be widely used to detect the dynamics of the fast-driven elastic object, as well as vortex matter, interacting with the substrates that may generate large heat.

By using this method, we determine the dynamic melting field $B^{\infty}_{c,dyn}(0)$ of the driven vortex lattice in a weak-pinning amorphous (a-)Mo_xGe_{1-x} film near $T = 0$. We construct an *ideal* vortex phase diagram in the *absence* of pinning, at $T = 0$ as a function of magnetic field B, which will be compared with the conventional one with weak pinning. Since the a-Mo_xGe_{1-x} film is a typical, conventional type-II superconductor with weak pinning, the results obtained in this work are helpful to understand the vortex states at low T for a variety of superconductors. More detailed data, analysis, and discussion have been given in Ref. [42].

2. Experimental details

An a-Mo_xGe_{1-x} film with thickness of 330 nm was fabricated by rf sputtering on a Si substrate held at room temperature [29-32]. The linear resistivity ρ and dc current-voltage $(I - V)$ characteristics were measured using a standard four-terminal method. The mean-field transition temperature T_{c0} defined by a 95% criterion of the normal-state resistivity [11, 12], $\rho(T_{c0}) = 0.95\rho_n$, and the zero-resistivity temperature T_c are 6.1 and 6.0 K, respectively. The equilibrium melting field $B_c(T)$ and the upper critical field $B_{c2}(T)$ are determined from $\rho(B_c) \to 0$ and $\rho(B_{c2}) = 0.95\rho_n$, respectively.

Figures 1(a) and (b) illustrate schematically the time evolution of the applied current I in the continuous-current mode used previously and the pulsed-current mode developed in this work, respectively. In the continuous mode, the dc current with fixed magnitude superimposed with the ac current I_{rf} is applied to the vortex system. The dc voltage V induced by the vortex motion is averaged over ten seconds and recorded. Then, the magnitude of the dc current I is increased in a step-by-step manner, as illustrated in figure 1(a). In the pulsed mode, on the other hand, the square pulse with duration of 1 ms is applied and its repetition time is set to 1 s, as shown in figure 1(b), which makes the duty ratio as small as 0.1 %. The voltage signal due to the vortex motion is again averaged over 10 s and recorded. In our ML measurement, the ac current I_{rf} with a frequency f_{ext} of up to 50 MHz is superimposed on the dc I pulse with 1 ms width. Hence, the number of cycles for superimposed I_{rf} should be adjusted depending on f_{ext}. For f_{ext} =50 MHz used in this work, for example, we apply I_{rf} over a duration of 50,000 cycles.

Figure 2 shows schematically the electrical circuit for the pulsed ML measurement, where the independent ac- and dc-pulse sources are used. The voltage enhanced with a preamplifier is recorded with a fast-Fourier transform (FFT) spectrum analyzer, which enables to measure $V(t)$

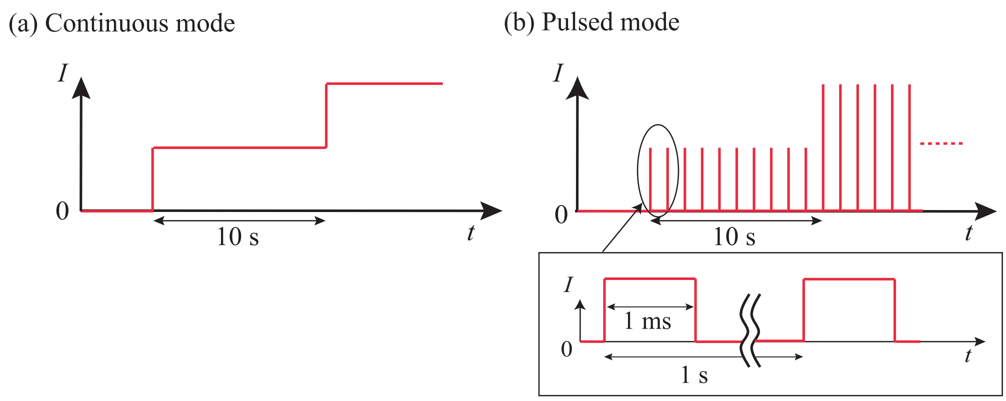

Figure 1. Schematic diagrams of the time evolution of the applied current I in (a) the continuous-current mode used conventionally and (b) the pulsed-current mode developed in this work, respectively. The ac current I_{rf} superimposed on I is not shown in (a) and (b). The lower diagram in (b) schematically illustrates the enlarged view of individual I pulses.

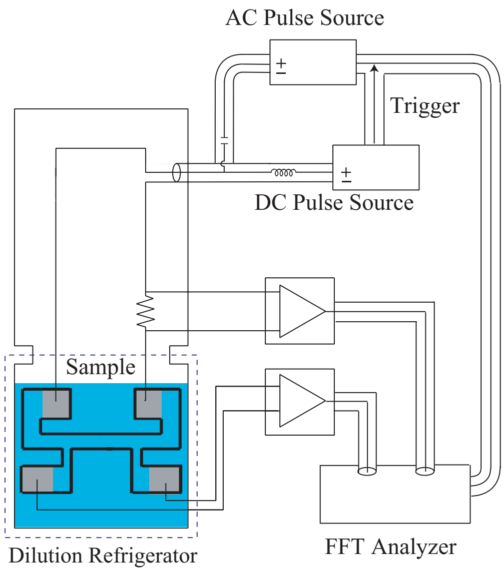

Figure 2. Schematic illustration of the electrical circuit used for the pulsed ML measurement.

with a voltage resolution as small as 0.01 mV. Since the time resolution of our FFT analyzer is 25 μs, the duration of the dc pulse should be longer than about 1 ms to ensure the accuracy of the ML measurement. The dc pulse is also used as a trigger signal to synchronize all the devices. In addition, we connect a capacitor and a coil with the ac and dc pulse sources, respectively, to prevent each pulse signal from penetrating the other pulse source.

Figures 3(a) and (b), respectively, show the set of waveforms for the voltage pulse $V(t)$ and current pulse $I(t)$ with different amplitudes superimposed with fixed 50 MHz I_{rf} measured in the pulsed current mode at 0.05 K in 8.0 T. Here, $I(t)$ of a given amplitude and corresponding $V(t)$ are indicated with the same color. A representative waveform of $V(t)$ selected from the data of figure 3(a) is shown in figure 3(c). The waveform of $V(t)$ as well as that of $I(t)$ exhibits a plateau-like behavior and hence $I-V$ characteristics are readily obtained from the plateau values. In the pulsed mode, the heat dissipated in the sample is estimated to be a few tens nW at around the first ML resonance step (see below). This leads to an increase in the local temperature of a few tens mK at 0.05 K [42], which will not affect the discussion that follows.

Now, we examine the experimental resolution of the ML measurement in the pulsed current mode in comparison with that in the continuous current mode. The solid and open circles in figure 4(a) show the dc I-V characteristics superimposed with 40 MHz I_{rf} at 4.1 K in 4.0 T, corresponding to OP near B_p, measured in the pulsed and continuous modes, respectively. Figure 4(b) displays $\mathrm{d}I/\mathrm{d}V$ versus V, where symbols correspond to those in figure 4(a). In this temperature and current-voltage range, heating effects caused by the vortex motion are negligibly small even if the continuous current mode is used. Figures 4(a) and (b) clearly show that the pulsed ML measurement yields the same result as the continuous one as long as the heating effects are not important and that the experimental resolution of ML in the pulsed mode is of the same level as that in the continuous mode [42].

3. Results and discussion

When a vortex lattice is driven at a given dc velocity v through a random pinning potential, it experiences a velocity modulation with a frequency f_{int} determined by the ratio of v to a lattice constant in the flow direction a, $f_{int} = v/a$ [41]. When the lattice is driven under the

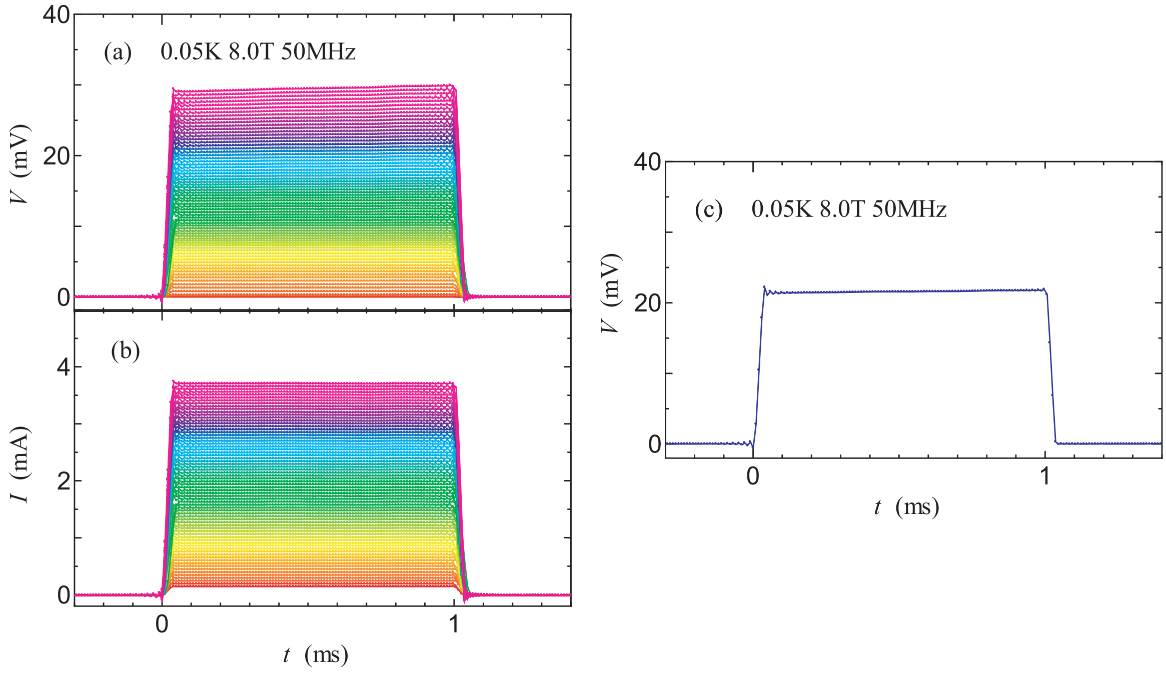

Figure 3. The set of waveforms for (a) the voltage pulse $V(t)$ generated by the vortex motion at 0.05 K in 8.0 T and (b) the current pulse $I(t)$ with different amplitudes on which 50 MHz I_{rf} with fixed amplitude is superimposed. Here, $I(t)$ of a given amplitude and corresponding $V(t)$ are indicated with the same color. (c) A typical waveform of $V(t)$ selected from the data in (a). All the waveforms show a plateau-like structure.

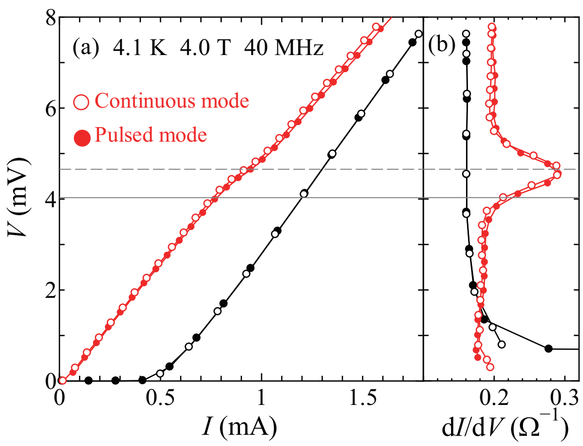

Figure 4. (a) Dc I-V characteristics at 4.1 K in 4.0 T measured in the pulsed (black solid circles) and continuous (black open circles) current modes, and those taken with superimposed 40 MHz I_{rf} in pulsed (red solid circles) and continuous (red open circles) current modes. (b) $\mathrm{d}I/\mathrm{d}V$ versus V, where symbols correspond to those in (a). Horizontal full and dashed lines mark the location of the ML resonance expected for the perpendicular and parallel orientations, respectively. Other lines are guides for the eye [42].

influence of externally applied dc and ac forces, a steplike structure analogous to Shapiro steps found in Josephson junctions appears in the $I-V$ characteristics [28-30,33-38], where I and V correspond to the dc driving force and the average velocity of vortices, respectively. The steps occur when the internal frequency $f_{int} = v/a$ of the system locks to the external frequency f_{ext} of the ac drive I_{rf} or when the relation $qf_{int} = pf_{ext}$ is satisfied, where p and q are integers.

If we assume a triangular vortex array, i.e., Abrikosov lattice, moving in the direction perpendicular to one side of the triangle(s), which we call the perpendicular orientation, we can calculate the value of the fundamental voltage step ($V_{p/q}^{perp}$) for a given B, satisfying the subharmonic resonant condition of $p/q = 1/2$, to be $V_{1/2}^{perp} = lf_{ext}(\sqrt{3}\Phi_0 B/2)^{1/2}$, where l is the distance between the voltage contacts and Φ_0 is the flux quantum [29, 31, 32, 36, 37]. The location of $V_{1/2}^{perp}$ is indicated by a full horizontal line in figures 4 and 5. When the vortex lattice is moving in the direction parallel to one side of the triangle(s), which we call the parallel orientation, the fundamental voltage step is calculated to be $V_{1/1}^{para} = (2/\sqrt{3})V_{1/2}^{perp}$. This is illustrated with a dashed horizontal line in figures 4 and 5. The observed ML resonance voltages in figures 4(a) and 4(b) nearly agree with the calculated values for the parallel orientation. This is consistent with previous work in which the lattice orientation favors the parallel one when the field is increased to around B_p [32, 43].

Let us present the data of the ML resonance acquired using pulsed currents at T =0.05 K, corresponding to $T/T_{c0} = 0.01$, which is the lowest temperature attained in this work. Figure 5(a) shows the I-V curves measured with superimposed 50 MHz I_{rf} of different amplitudes listed in the figure (I_{rf} = 0.31 - 2.77 mA) at 0.05 K in 8.0 T, which corresponds to OP prior to

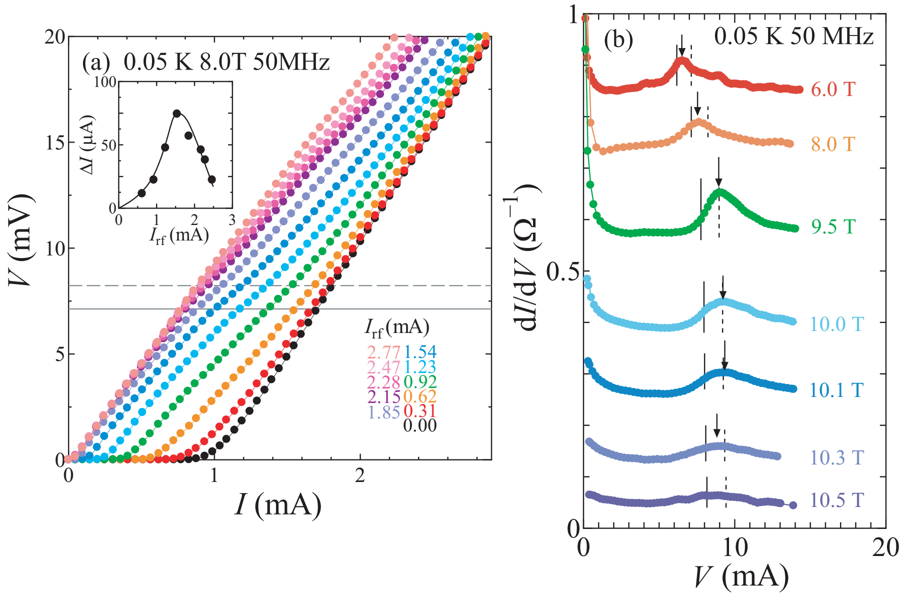

Figure 5. (a) I-V curves at 0.05 K in 8.0 T taken with superimposed 50 MHz I_{rf} of different amplitudes listed in the figure. Black circles represent the I-V data measured in the absence of superimposed I_{rf}. The location of $V_{1/2}^{perp}$ and $V_{1/1}^{para}$ is indicated with horizontal full and dashed lines, respectively. Inset: ΔI plotted as a function of I_{rf}. (b) dI/dV versus V curves measured with superimposed 50 MHz I_{rf} for different B [42]. A short arrow marks the location of the observed ML peak at each B. Short full and dashed lines indicate the location of $V_{1/2}^{perp}$ and $V_{1/1}^{para}$, respectively.

B_p(≈10 T). Black circles depict the I-V data taken in the absence of superimposed I_{rf}, showing the smooth curvature. In the presence of superimposed I_{rf}, by contrast, we observe the step-like structure at around a voltage marked with a horizontal full line. Here, the location of the calculated $V_{1/2}^{perp}$ and $V_{1/1}^{para}$ is indicated with the horizontal full and dashed lines, respectively. The ML resonance is more clearly seen by plotting dI/dV against V, as shown in figure 5(b). To quantify the strength of the ML resonance, we extract the width of the current step ΔI at the ML resonance in the I-V characteristics by integrating the peak of dI/dV versus V curves with respect to the flux-flow baseline [31, 32, 36, 37]. As shown in the inset of figure 5(a), thus obtained ΔI exhibits a maximum as a function of I_{rf}, consistent with earlier work that $\Delta I(I_{rf})$ is given by a squared Bessel function of the first kind [28, 36]. In the following discussion, we will deal with the data corresponding to the maximum resonance ΔI_{max}.

Now, we focus on the field dependence of the ML resonance at 0.05 K. Shown in figure 5(b) are the dI/dV versus V curves measured with superimposed 50 MHz I_{rf} for different B. Short vertical full and dashed lines represent the location of $V_{1/2}^{perp}$ and $V_{1/1}^{para}$ expected for the perpendicular and parallel orientations, respectively. A short arrow marks the position of the observed ML peak in individual fields indicated in the figure. The peak structure is visible over the broad B up to about 10.3 T but vanishes at $B \gtrsim$10.5 T. By plotting ΔI_{max} against B, we find that at both 0.05 and 0.4 K, ΔI_{max} takes a sharp peak around B_p (≈10 T) and rapidly falls to zero at a certain field just above B_p [42]. The sharp peak structure in ΔI_{max} found around near B_p implies the temporal recovery of the ML resonance, which is most likely attributed to the growth in the portion of the ordered domains with parallel orientation [43]. The subsequent sudden drop in ΔI_{max} shows the rapid collapse of the lattice order, indicating a sharp melting from a moving lattice into a moving liquid. To identify the dynamic melting field $B_{c,dyn}$ at each temperature, we determine $B_{c,dyn}$ from a simple linear extrapolation of ΔI_{max} to zero. Then, we evaluate the dynamic melting field $B_{c,dyn}^{\infty}$ in the limit of the infinite velocity ($v \to \infty$) as a field at which f_{ext}^{-1} versus $B_{c,dyn}(f_{ext})$ extrapolates linearly to $f_{ext}^{-1} \to 0$. Thus obtained values of $B_{c,dyn}^{\infty}$ at 0.05 and 0.4 K are 10.5 and 10.4 T, respectively.

By plotting $B_{c,dyn}^{\infty}(T)$ and $B_{c2}(T)$ in the $B-T$ plane, we now complete the dynamic as well as the static vortex phase diagram over the entire B and T range [42]. From a simple extrapolation of the $B_{c,dyn}^{\infty}(T)$ curve to $T = 0$, we are able to obtain $B_{c,dyn}^{\infty}(0)$, as well as $B_p(0)$, $B_c(0)$ and $B_{c2}(0)$, thus constructing the phase diagram of an *ideal* vortex system *without* pinning at $T = 0$ as a function of B. This is illustrated in figure 6(a). For comparison, the similar $T = 0$ phase

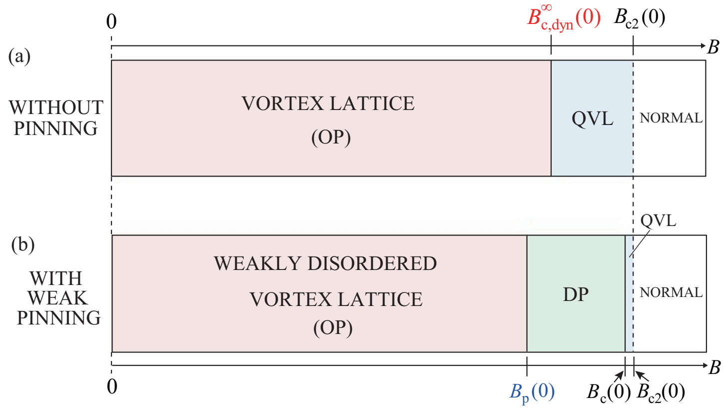

Figure 6. (a) The $T = 0$ equilibrium phase diagram with respect to B for an ideal vortex system without pinning and (b) that in an actual system with weak pinning [42].

diagram for a real system with weak pinning, which is constructed based on the data of $B_p(T)$, $B_c(T)$, and $B_{c2}(T)$ at $T \to 0$, is shown in figure 6(b).

From figures 6(a) and (b), one can trace how the equilibrium phase diagram for the ideal pinning free system alters as a small amount of pinning centers is introduced into the system. In the absence of pinning, only the vortex-lattice phase (OP) and the vortex-liquid phase exist, where the melting field of the vortex lattice is identified as $B^{\infty}_{c,dyn}(0)$ and the vortex-liquid phase at $T \to 0$ is considered to be a quantum vortex liquid (QVL) [11, 12]. When the weak pinning centers are introduced into the system, DP (or the vortex-glass phase) emerges just above OP. The upper bound of OP is slightly suppressed from $B^{\infty}_{c,dyn}(0) = 10.5$ T to $B_p(0) = 10.0$ T, indicative of pinning-induced disordering of the vortex lattice. On the other hand, the "melting" field between the vortex solid phase (DP) and the QVL phase is remarkably pushed up from $B^{\infty}_{c,dyn}(0) = 10.5$ T to $B_c(0) = 12.4$ T, leading to a significant suppression of the QVL phase. This result is explained in terms of the enhanced pinning effect at low T. We have indeed found that at high temperatures ($T \gtrsim 3$ K), $B^{\infty}_{c,dyn}(T)$ is very close to $B_c(T)$. This is because at high T, thermal-fluctuation effects on vortex pinning are so strong that the melting field $B^{\infty}_{c,dyn}(T)$ in the absence of pinning stays almost unaffected by the introduction of a small amount of pinning.

4. Conclusion

We have developed and presented the pulsed ML measurement that generates much less heat than the conventional one and successfully determined the dynamic melting field $B^{\infty}_{c,dyn}(T)$ of the driven vortex lattice for the thick a-Mo_xGe_{1-x} film in the limit $T \to 0$ and infinite velocity $v \to \infty$. From the dynamic as well as equilibrium $B - T$ phase diagram at low T, we have mapped out an ideal vortex phase diagram in the absence of pinning, at $T \to 0$ as a function of B. We hope that the pulsed ML technique developed and detailed in this paper may be widely used to explore the dynamics of the fast driven vortex matter and elastic objects interacting with random substrates that may generate large heat.

Acknowledgments

This work was supported by a Grant-in-Aid for Scientific Research from the Ministry of Education, Culture, Sports, Science, and Technology of Japan. A. O. acknowledges the financial support from the Global Center of Excellence Program by MEXT, Japan through the "Nanoscience and Quantum Physics" Project of the Tokyo Institute of Technology.

References

[1] Blatter G, Ivlev B, Kagan Y, Theunissen M, Volokitin Y and Kes P 1994 *Phys. Rev.* B **50** 13013
[2] Blatter G and Ivlev B 1993 *Phys. Rev. Lett.* **70** 2621
[3] Fisher M P A 1990 *Phys. Rev. Lett.* **65** 923
[4] Ikeda R 1996 *Int. J. Mod. Phys.* B **10** 601
[5] Myojin K, Ikeda R and Koikegami S 2008 *Phys. Rev.* B **78** 014508
[6] Chudnovsky E M 1995 *Phys. Rev.* B **51** 15351
[7] Rozhkov A and Stroud D 1996 *Phys. Rev.* B **54** R12697
[8] Chervenak J A and Valles Jr J M 1996 *Phys. Rev.* B **54** R15649
[9] Sasaki T, Biberacher W, Neumaier K, Hehn W, Andres K and Fukase T 1998 *Phys. Rev.* B **57** 10889
[10] Shibauchi T, Krusin-Elbaum L, Blatter G and Mielke C H 2003 *Phys. Rev.* B **67** 064514
[11] Okuma S, Imamoto Y and Morita M 2001 *Phys. Rev. Lett.* **86** 3136
[12] Okuma S, Togo S and Morita M 2003 *Phys. Rev. Lett.* **91** 067001
[13] Bustarret E, Kačmarčik J, Marcenat C, Gheeraert E, Cytermann C, Marcus J and Klein T 2004 *Phys. Rev. Lett.* **93** 237005
[14] Taylor B J, Scanderbeg D J, Maple M B, Kwon C and Jia Q X 2007 *Phys. Rev.* B **76** 014518
[15] Taylor B J and Maple M B 2007 *Phys. Rev.* B **76** 014517
[16] Kuwasawa Y, Kato K, Matsuo M and Nojima T 1998 *Physica* C **305** 95
[17] Saito Y, Nojima T and Iwasa Y 2016 *Supercond. Sci. Technol.* **29** 093001
[18] Okuma S, Kashiro K, Suzuki Y and Kokubo N 2008 *Phys. Rev.* B **77** 212505

IOP Conf. Series: Journal of Physics: Conf. Series **871** (2017) 012022 doi:10.1088/1742-6596/871/1/012022

[19] Paltiel Y *et al.* 2000 *Phys. Rev. Lett.* **85** 3712
[20] Paltiel Y *et al.* 2000 *Nature* **403** 398
[21] Kes P H and Tsuei C C 1983 *Phys. Rev.* B **28** 5126
[22] Bhattacharya S and Higgins M J 1993 *Phys. Rev. Lett.* **70** 2617
[23] Marley A C, Higgins M J and Bhattacharya S 1995 *Phys. Rev. Lett.* **74** 3029
[24] Ghosh K *et al.* 1996 *Phys. Rev. Lett.* **76** 4600
[25] Rosenstein B and Zhuravlev V 2007 *Phys. Rev.* B **76** 014507
[26] Bermúdez M M, Eskildsen M R, Bartkowiak M, Nagy G, Bekeris V and Pasquini G 2015 *Phys. Rev. Lett.* **115** 067001
[27] Guillamón I, Córdoba R, Sesé J, De Teresa J M, Ibarra M R, Vieira S and Suderow H 2014 *Nat. Phys.* **10** 851
[28] Schmid A and Hauger W 1973 *J. Low Temp. Phys.* **11** 667
[29] Kokubo N, Asada T, Kadowaki K, Takita K, Sorop T G and Kes P H 2007 *Phys. Rev.* B **75** 184512
[30] Okuma S, Inoue J and Kokubo N 2007 *Phys. Rev.* B **76** 172503
[31] Okuma S, Imaizumi H and Kokubo N 2009 *Phys. Rev.* B **80** 132503
[32] Okuma S, Imaizumi H, Shimamoto D and Kokubo N 2011 *Phys. Rev.* B **83** 064520
[33] Fiory A T 1971 *Phys. Rev. Lett.* **27** 501
[34] Higgins M J, Middleton A A and Bhattacharya S 1993 *Phys. Rev. Lett.* **70** 3784
[35] Reichhardt C, Scalettar R T, Zimányi G T and Grϕnbech-Jensen N 2000 *Phys. Rev.* B **61** R11914
[36] Kokubo N, Kadowaki K and Takita K 2005 *Phys. Rev. Lett.* **95** 177005
[37] Okuma S, Shimamoto D and Kokubo N 2012 *Phys. Rev.* B **85** 064508
[38] Reichhardt C and Olson Reichhardt C J 2015 *Phys. Rev.* B **92** 224432
[39] Koshelev A E and Vinokur V M 1994 *Phys Rev. Lett.* **73** 3580
[40] Olson C J, Reichhardt C and Nori F 1998 *Phys. Rev. Lett.* **81** 3757
[41] Togawa Y, Abiru R, Iwaya K, Kitano H and Maeda A 2000 *Phys. Rev. Lett.* **85** 3716
[42] Ochi A, Sohara N, Kaneko S, Kokubo N and Okuma S 2016 *J. Phys. Soc. Jpn.* **85** 044701
[43] Zhuravlev V and Maniv T 2006 *Europhys. Lett.* **73** 955